High-Speed Imaging of Rab Family Small GTPases Reveals Rare Events in Nanoparticle Trafficking in Living Cells
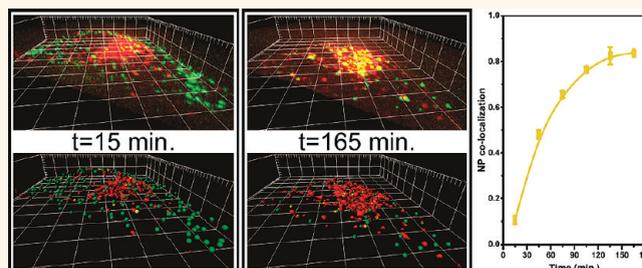
Peter Sandin,[†,*] Laurence W. Fitzpatrick,[†] Jeremy C. Simpson,[‡] and Kenneth A. Dawson[†,*]

[†]Centre for BioNano Interactions, School of Chemistry and Chemical Biology & UCD Conway Institute of Biomolecular and Biomedical Research and [‡]School of Biology and Environmental Science & UCD Conway Institute of Biomolecular and Biomedical Research, University College Dublin, Belfield, Dublin 4, Ireland

Due to their potential as tools to improve diagnosis and treatment of diseases, engineered nanoparticles (NPs) have received much attention in recent years. However, despite significant efforts, considerable uncertainties remain about the mechanisms by which NPs are taken up and trafficked in cells (for recent reviews summarizing published data as well as discussing different approaches currently employed, see refs 1–6). Studies on the endocytic mechanisms potentially used have shown NP uptake to be dependent on NP size,[7–9] shape,[7,10] surface,[8,10–12] and cell type.[11–14] On the other hand, studies on intracellular trafficking have shown that most NPs, irrespective of shape, charge, and size, accumulate in the lysosomes, although there are examples indicating that NP escape from this degradative pathway is possible.[9,11,15,16] To date, most studies have focused on identifying the point of entry and final destination; however, for NPs to meet their promise in the field of nanomedicine, delivery to desired organs and cell types will not be adequate, but rather the ability to target specific subcellular compartments will be needed. To realize this, a deeper knowledge and understanding of the entire intracellular itinerary will be essential, and in the nanomaterial and NP field, this is a considerable challenge. Unlike biomolecules, NPs can be constructed from a wide variety of materials, therefore making their surfaces notoriously heterogeneous in structure, in turn resulting in a diversity of biological molecules (their biomolecular corona) that can be bound to them.[17–20] It is, in principle, possible that the original corona, combined with new molecules picked up inside the cell, could, even if rarely, provide the NPs with signals to allow them to access different subcellular destinations. Studies addressing this critical concept have commonly used fluorescence microscopy on fixed cells to analyze cellular localization and distribution of NPs. However, clearly such approaches will only ever provide a snapshot representing their bulk movement inside the cell. This will mean that minor, but potentially important, subpopulations of NPs will be overlooked. In addition, such approach is also known to potentially cause fixation artifacts, particularly in regard to spatial organization and distribution.[21]

ABSTRACT

Despite the increased application of nanomaterials in diagnostics and therapeutics, methods to study the interactions of nanoparticles with subcellular structures in living cells remain relatively undeveloped. Here we describe a robust and quantitative method that allows for the precise tracking of all cell-associated nanoparticles as they pass through endocytic compartments in a living cell. Using rapid multicolor 3D live cell confocal fluorescence microscopy, combined with transient overexpression of small GTPases marking various endocytic membranes, our studies reveal the kinetics of nanoparticle trafficking through early endosomes to late endosomes and lysosomes. We show that, following internalization, 40 nm polystyrene nanoparticles first pass through an early endosome intermediate decorated with Rab5, but that these nanoparticles rapidly transfer to late endosomes and ultimately lysosomes labeled with Rab9 and Rab7, respectively. Larger nanoparticles of 100 nm diameter also reach acidic Rab9- and Rab7-positive compartments although at a slower rate compared to the smaller 40 nm nanoparticles. Our work also reveals that relatively few nanoparticles are able to access endocytic recycling pathways, as judged by lack of significant colocalization with Rab11. Finally, we demonstrate that this quantitative approach is sufficiently sensitive to be able to detect rare events in nanoparticle trafficking, specifically the presence of nanoparticles in Rab1A-labeled structures, thereby revealing the wide range of intracellular interactions between nanoparticles and the intracellular environment.

KEYWORDS: nanoparticles · membrane traffic · Rab GTPases · intracellular trafficking · colocalization · live cell imaging · polystyrene particles

©2012 American Chemical Society
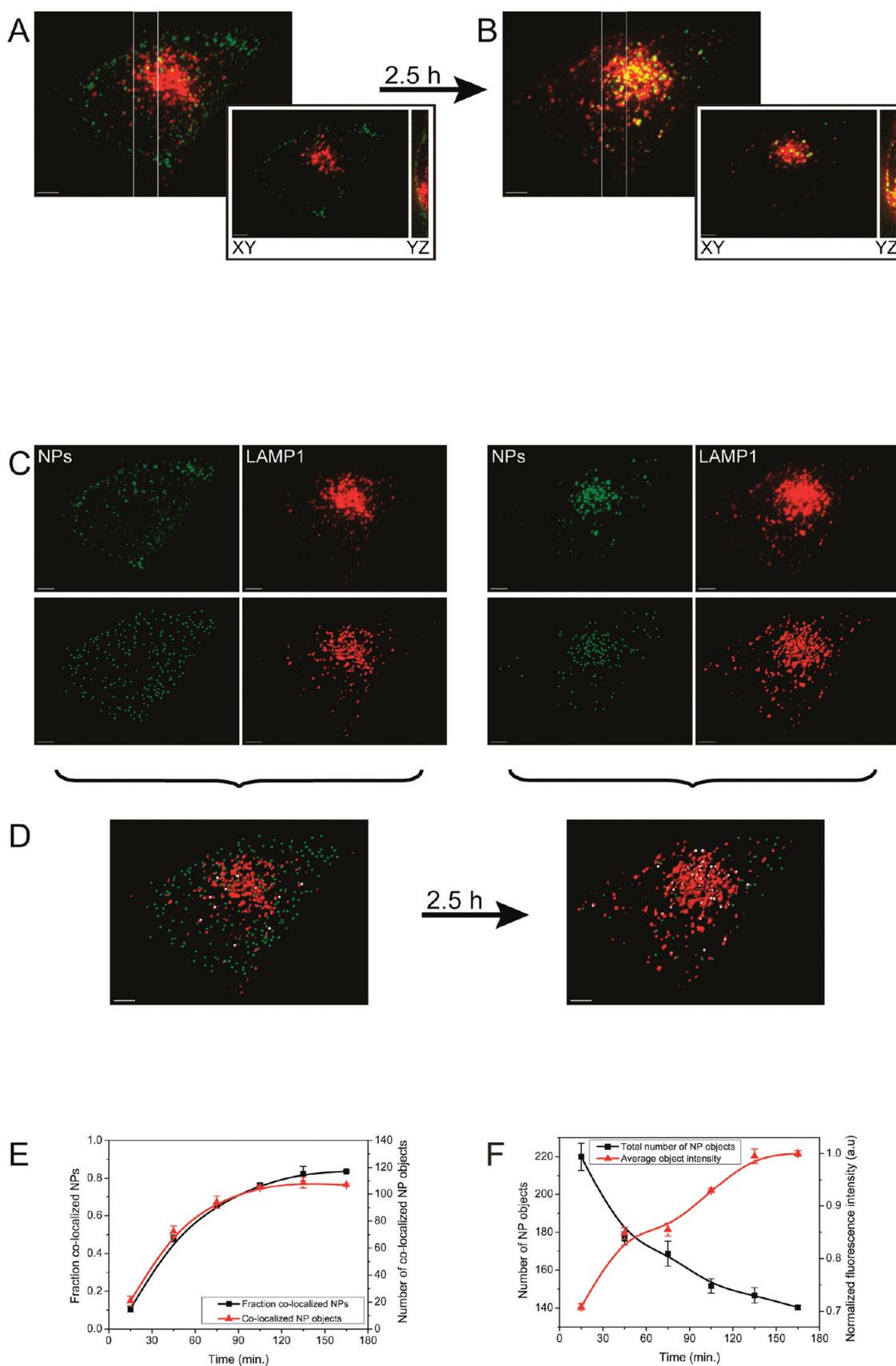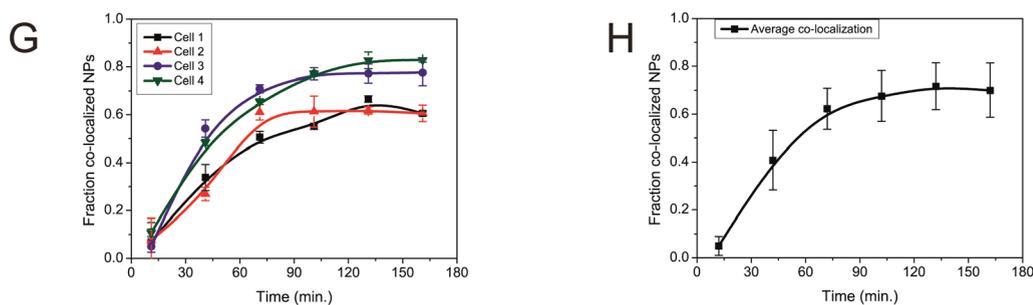
Figure 1. Quantitative analysis of 40 nm NP uptake and intracellular transport to LAMP1-labeled organelles over time. (A,B) Masked out maximum intensity projections (MIPs) of representative 3D images of a transiently transfected HeLa cell immediately after (~15 min) a short pulse of NPs, and 2 h and 45 min later (NPs in green and LAMP1-RFP in red). Insets show the *XY* and *YZ* slices of the images in (A) showing the NPs being mainly located at the cell surface at the first time point, and then in the juxta-nuclear region after almost 3 h of chase. (C) Illustration of the segmentation of the masked cells. The upper row shows the MIPs of the NPs and LAMP1-RFP for the first and last time points. The lower row shows the corresponding segmented, digitized images. (D) Merge of the segmented NPs and LAMP1-RFP in (C) showing the colocalized NPs in white. All scale bars represent 5 μm. (E) Time-dependent colocalization expressed as both the fraction of the cell-associated NPs that colocalize with LAMP1 structures (black) and as the absolute number of colocalized NP objects (red). (F) Changes over time in total numbers of cell-associated NP objects (black) and their average fluorescence intensity (red). (G,H) Time-dependent colocalization profiles for four individual cells as separate graphs (G) and averaged over all four cells (H). In (E–G), each time point shows the average of the three consecutive frames acquired. In (H), each time point is the average of the three frames and the four cells resulting in a total of 12 3D frames being averaged. The error bars in all cases represent the standard deviation of the averaged frames.

In order to address this deficiency, we employ rapid time-lapse confocal imaging of nanoparticles in living cells, in which we label various intracellular membranes with fluorescent reporters. Rather than relying on the use of potentially biased and limited fixed-cell colocalization coefficients, our approach takes advantage of both the spatial and the temporal information that can be gained from using living cells. Specifically, we consider the correlated co-movement of colocalized structures and thereby provide enhanced confidence in the colocalization metrics obtained. The recent technical advances in fluorescence microscopy and fluorescent probes for live cells are making this possible, and reports using the temporal and spatial information to determine colocalization between NPs and intracellular compartments are beginning to emerge.[22] An additional key feature of the present approach is the use of high-speed spinning disk confocal fluorescence microscopy combined with piezo technology for fast z-sectioning. This allows us to capture 3D snapshots of the entire cell and follow individual cells over an extended period of time. Furthermore, imaging the entire volume of the cell allows us to follow all cell-associated NPs, which is of importance if we are to capture rare, but potentially significant, events.

RESULTS AND DISCUSSION

As a model system to test our methodology, we chose a well-characterized NP, specifically, fluorescently labeled 40 nm carboxylated polystyrene (for size and z-potential, see Supporting Information Table S1) and HeLa cells. It has previously been shown, by us and others, that following internalization these NPs ultimately accumulate in lysosomes;[9,15,23] however, the molecular nature of the endocytic organelle intermediates through which they pass has not been fully elucidated.

Initially, we labeled the cells with the well-known lysosomal resident, lysosomal-associated membrane protein 1 (LAMP1) fused to RFP. The cells were exposed to a 1 min pulse of NPs after which they were imaged every 30 min up to a maximum of 3 h after NP addition. At each time point, three consecutive, full 3D images of the entire cell were captured (approximately 7–10 s per frame) and then processed using image analysis software (see Materials and Methods). Inspection of both maximum intensity projections and single image slices (Figure 1A,B) revealed that at early time points the NPs displayed a largely peripheral localization pattern, but on incubation, this changed to a juxta-nuclear distribution. In order to make our analysis quantitative, we next applied an object-based colocalization analysis protocol (for details, see Materials and Methods). Briefly, fluorescent objects in the 3D images were segmented (Figure 1C), creating a digitized representation of both NPs and LAMP1-positive structures (Figure 1D). Using this image, we determined which NP objects were localized within LAMP1-positive structures (Figure 1D). For each time point, the data extracted from the three consecutive 3D images were averaged in order to reduce the contribution of false colocalization values caused by close spatial proximity. The colocalization was calculated both as the fraction of cell-associated NPs that colocalize with LAMP1-labeled structures and also simply as the number of colocalized "NP objects". We use NP objects since the objects identified as NPs when segmenting the images may contain one or several NPs, thus, referring to them as NPs could be misleading. When calculating the fraction of colocalized NPs, the intensity data for the NP objects were used to obtain a value that reflected the actual number of NPs. Quantification revealed a gradual increase in the colocalization of
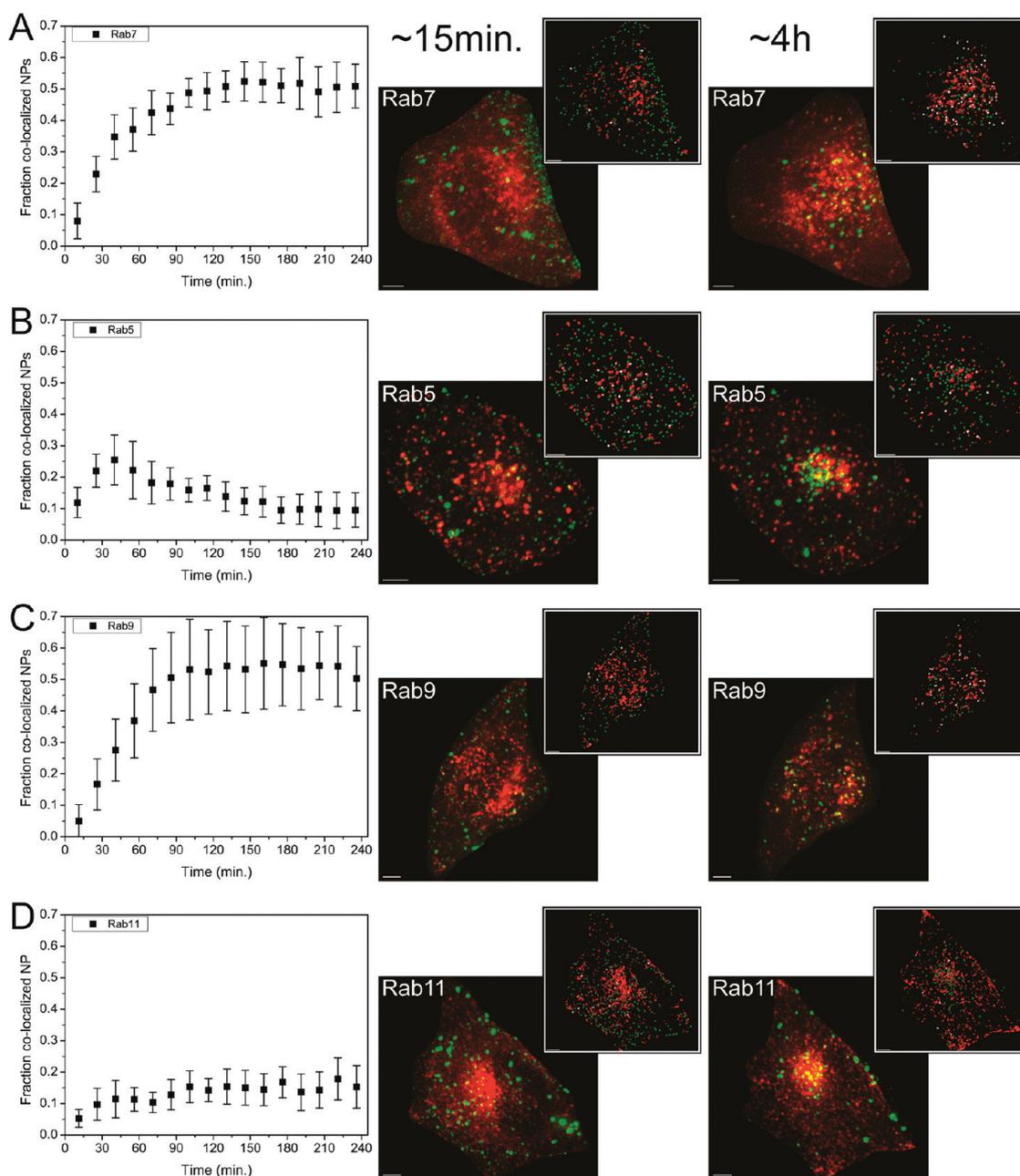
Figure 2. Time profiles of colocalization between 40 nm NPs and Rab7 (A), Rab5 (B), Rab9 (C), and Rab11 (D) together with representative MIP images of the HeLa cells at the first (~15 min) and final time points (~4 h). The colocalization values are given as the fraction of cell-associated NPs colocalizing with each Rab. Each time point is an average of three consecutive frames from five different cells (for individual traces, see Supporting Information Figure S1), and the error bars indicate the standard deviation between cells. The images show both the masked out raw and the corresponding segmented, digitized image. NPs are shown in green, Rab structures are shown in red, and in the segmented image, the colocalizing NP objects are shown in white. All scale bars represent 5 μm.

NPs with LAMP1 over the first 90 min, reaching a maximum value of 80%, after which time the degree of colocalization remained constant (Figure 1E). In addition to providing an accurate measurement of colocalization, our method also allowed us to extract additional information about the internalization of the NPs into cells, including the total number of cell-associated NP objects and their fluorescence intensity (Figure 1F). These data provide an alternative means,

but independent of the colocalization method, to measure the intracellular accumulation of the same population of NPs. These analyses revealed a rapid decrease of the number of NP objects, presumably as a result of endosome fusion events, accompanied by an increase in their fluorescence intensities over time (Figure 1F). We next applied our analysis method to more cells within the population in order to evaluate the reproducibility of the measurements. Results from

four independent cells revealed very similar colocalization profiles across all the cells (Figure 1G,H), with the kinetics of lysosomal accumulation being in good agreement with other reported studies.[9,15,23,24] Interestingly, although these experiments revealed an overall steady increase in the accumulation of NPs in lysosomes, the transfer rates of individual NP objects to lysosomes were highly heterogeneous. Indeed, we observed NPs colocalizing with LAMP1-positive structures as early as 15 min after the NP pulse, but equally in some cells, there were also NPs seemingly still on the cell membrane after 3 h (Figure 1A,B and Supporting Information video S1).

These initial results confirmed the validity of our approach and provided us with an experimental platform with which to explore in greater detail the pathway taken by NPs from cell surface to lysosomes. The transfer of cargo between membrane organelles of the endocytic pathway is a complex process involving multiple intermediates and a wide variety of trafficking machinery molecules.[25,26] Indeed, it still remains to be clarified whether transport to lysosomes is a process driven by organelle maturation or simple budding and fusion events.[27] Nevertheless, what has become clear is that one of the major classes of proteins regulating all intracellular traffic is the Rab family of small GTPases.[28] In humans, there are approximately 60 known members of this family, each with a specific localization profile. Furthermore, Rabs not only function as components of the core trafficking machinery but they also seem to provide specific identity to the organelles to which they are bound.[29] Previous studies have utilized fluorescently tagged Rab proteins as organelle markers and determined that Rab subdomains, on endosomal compartments in particular, provide molecular platforms through which cargo is sorted.[30] All membrane structures participating in trafficking events are likely to contain at least one Rab family member, and therefore, we hypothesized that, by studying the co-movement of NPs with various Rabs, we would be able to precisely establish the complete intracellular pathway taken by NPs.

In order to explore this approach, we transfected cells with various constructs encoding fluorescently tagged Rab proteins associated with endosomal—lysosomal trafficking. For our initial studies, we transfected cells with a construct encoding mCherry-Rab7, a small GTPase essential for the maturation of late endosomes, and fusion with lysosomes.[31,32] These cells were exposed to a 1 min pulse of NPs, followed by a chase in NP-free medium during which time the cells were imaged every 15 min for up to 4 h. A total of five cells, from two independent experiments, were analyzed and averaged (Figure 2A; for the time traces of each individual cell, see Supporting Information Figure S1). Strikingly, the time-dependent colocalization profile between NPs and Rab7 was almost indistinguishable

from that observed between NPs and LAMP1 (Figure 1H), both showing a steady increase in colocalization up to 90 min after which time the level of colocalization remained constant.

We therefore extended our analysis across a number of other relatively well-characterized Rab GTPases, namely, Rab5A, Rab9A, and Rab11A, all associated with various endocytic compartments.

Using the same approach as for Rab7, the time-dependent colocalization between the NPs and each of the fluorescently tagged Rab proteins in turn was investigated, revealing a variety of colocalization profiles (Figure 2B—D; for graphs of each individual cell, see Supporting Information Figure S1). Rab5A mediates endocytosis and early endosome fusion and is found on early endosomes, phagosomes, caveosomes, and the plasma membrane and is generally considered as the first Rab encountered during the internalization process.[28,33] In Rab5-overexpressing cells, we observed an initial increase in colocalization of the NPs with this early endosome marker, peaking at 45 min after NP internalization, followed by a decline in colocalization to background levels (Figure 2B). This suggests a transient occupancy of the NPs in Rab5-labeled membranes, most likely classical early endosomes, before their release into other endocytic intermediates. Rab9 plays a role in the organization of late endosomes and the recycling of acid hydrolase receptors from late endosomes to the *trans*-Golgi network (TGN).[34] The colocalization profile with Rab9 was clearly different to that observed with Rab5; however, it was highly similar to that of Rab7, with an initial rapid increase followed by a plateau (Figure 2C). Although Rab9 plays a specific role in returning mannose-6-phosphate receptors from late endosomes back to the TGN, it also functions as a general organizer of late endosome subdomains.[35] The fact that we observed a steady increase in colocalization of NPs with this marker, coincident with a decline in the colocalization with Rab5, could suggest that NPs are sequentially passaged through Rab5-positive followed by Rab9-positive intermediates en route to the lysosomes. Furthermore, the fact that we did not observe a decline in colocalization between NPs and Rab9 up to 4 h after NP internalization suggests that, in addition to Rab7-positive membranes, NPs become trapped in Rab9-positive structures. Finally, we examined the colocalization of the NPs with Rab11A (Figure 2D). These experiments revealed a consistently low degree of colocalization, always below 18% between NPs and this endocytic marker. In nonpolarized cells, Rab11A is associated with endocytic recycling,[36] so our lack of detection of significant amounts of NPs in Rab11-positive membranes suggests that NPs of this type are not easily retrieved from the degradative pathway. This is consistent with other reports that show that release of nanoparticles from cells is an uncommon process.[23,24,37,38]
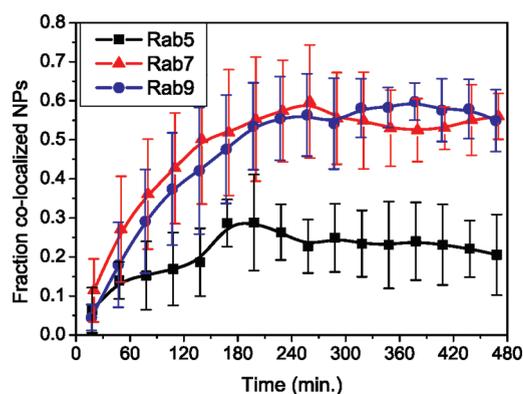
Figure 3. Time-dependent colocalization between 100 nm NPs and Rab5- (black), Rab7- (red), and Rab9- (blue) labeled structures. The colocalization value is expressed as the fraction of cell-associated NPs colocalizing with each respective Rab. Each time point is an average of three consecutive frames from five different cells (for individual traces, see Supporting Information Figure S2), and the error bars indicate the standard deviation between cells.

So far, our studies have focused on the internalization pathway taken by 40 nm carboxylated polystyrene NPs. In order to see whether the colocalization profiles that we observed for this particular nanoparticle were a general phenomenon, we also investigated the uptake profile of 100 nm carboxylated polystyrene NPs. Similar to the results obtained for the 40 nm NPs, these larger particles also showed a steady increase in colocalization with Rab7 and Rab9 (Figure 3), although the plateau occurred significantly later after internalization, at approximately 180 min, compared to 90 min for the 40 nm NPs (Figure 2A). However, in experiments in Rab5-overexpressing cells, we observed no sharp transient accumulation of NPs in these membranes, but rather a very gradual increase in colocalization with this marker, peaking at 180 min after internalization (Figure 3). Additionally, when comparing the individual time traces for the 100 nm NPs and Rab5 (see Supporting Information Figure S2), no common trend, when compared to the 40 nm NPs, was identifiable. Together, these results suggest that although the 100 nm NPs, similar to the 40 nm NPs, eventually accumulate in Rab9- and Rab7-positive compartments, there may be differences in the early trafficking events that transfer them from the plasma membrane, before reaching a common acidic endosome. This is also consistent with the view that 40 nm NPs are subjected to clathrin-mediated endocytosis (a process itself involving Rab5), compared to the larger particles that may use an alternative mechanism to transit the plasma membrane.[9] The possibility exists that, for these larger NPs, the internalization and trafficking steps are more heterogeneous in nature, as a reduced number of NPs at any one time would be able to occupy Rab5-labeled compartments, compared to the case with smaller NPs. An additional possibility worth consideration is that these larger particles may have a requirement for additional
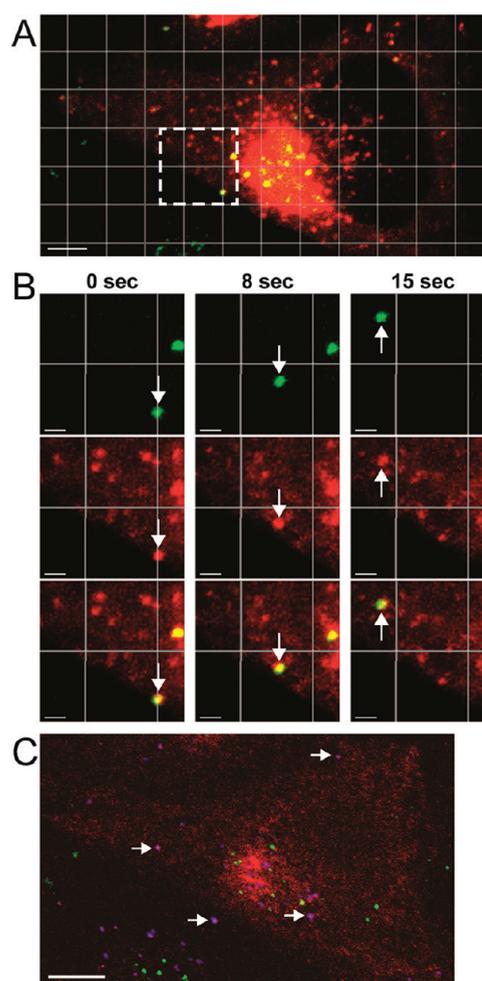

Figure 4. (A) Single frame from a live cell movie showing a HeLa cell expressing mCherry-Rab1A (red), approximately 4.5 h after being exposed to 40 nm carboxylated polystyrene NPs (green). The figure shows the maximum intensity projection (MIP) of five optical slices. (B) Three frames from the time-lapse video sequence (Supporting Information video S2) showing co-movement between NPs and Rab1A-decorated vesicles. The frames are enlargements of the area indicated by the dashed square in (A). Upper, middle, and lower rows show the NPs, Rab1A, and the merge, respectively. (C) Confocal image of the same cell following fixation and immunostaining with anti-LC3 antibodies (blue). NPs are shown in green, and mCherry-Rab1A is shown in red. The colocalization between LC3 and mCherry-Rab1A appears as magenta, with colocalizing structures indicated by arrows. The scale bars represent (A) 5 μm, (B) 2 μm, and (C) 7 μm.

trafficking factors to be recruited, in turn requiring specific gene expression events. Further systematic analysis of the internalization process taken by various classes on NPs, and indeed gene expression profiling, would be needed to fully understand and explain these observations.

Finally, we decided to challenge the sensitivity of our system by investigating whether we could observe the presence of NPs in membranes decorated with Rabs not generally associated with endocytic function. To this end, we selected Rab1A, one of the first identified members of the Rab family. Rab1A has a

well-established localization at endoplasmic reticulum (ER) exit sites and the pre-Golgi intermediate compartment (IC), where it mediates an essential role in ER-to-Golgi trafficking.[39] Strikingly, we were consistently able to detect clear co-movement between the NPs and Rab1A-labeled vesicles in the majority of transfected cells analyzed (Figure 4 and Supporting Information video S2). The fact that we were able to detect these colocalization events as early as 30–60 min after NP internalization argues against the complete retrograde routing of NPs from cell surface through endosomes and the Golgi complex. Furthermore, we were unable to detect colocalization between NPs and the COPI coat complex (data not shown), a multisubunit protein assembly present on ER-Golgi transport intermediates.[40] Another possibility is therefore that Rab1 may display an alternative, albeit minor, localization profile in cells treated with NPs. Recently, Zoppino and colleagues have reported a function for Rab1B, a closely related isoform of Rab1A in autophagy and autophagosome formation.[41] Autophagy is a process that can be induced in cells to degrade specific organelles in a controlled manner in response to stress. In our NP-treated cells, we were able to detect numerous membrane structures that were labeled with both Rab1A and LC3 (a key autophagy regulator); however, these membranes never contained NPs (Figure 4C). Although our experimental approach cannot formally exclude that autophagy is occurring in our cells, and indeed others have reported that autophagy can be induced by NPs,[42] at least at this particular time point after internalization, we were not able to detect such events.

Nevertheless, our observations of membranes labeled with Rab1A and containing nanoparticles were highly reproducible, as we were able to clearly detect these colocalizing and co-moving structures in many of the cells examined. Recently, a new role for Rab1A in regulating the motility of early endocytic vesicles has been reported[43] which could explain the co-movement we detect. However, it is puzzling that the co-movement is significant even 4–5 h after the NP pulse, a time at which most NPs have been passaged through the early endosomal compartments and have been delivered to the lysosomes. Clearly more work will be needed to further understand the role of these membranes in NP trafficking. Nevertheless, the approach and specific data that we present here highlight the power of quantitative live cell imaging in detecting the range of intracellular compartments that can be accessed by NPs.

CONCLUSIONS

In summary, we have developed a novel, highly sensitive, and quantitative approach to elucidate the precise nature of membrane compartments through which NPs are routed following internalization into cells. This methodology is particularly powerful as it has been applied in living cells, allowing us to follow in real time the relationship between NPs and various endocytic intermediates, providing a comprehensive overview of the complete particle trafficking profile. Additionally, this technology can be applied to study colocalization of particles with any cellular marker for which a fluorescently tagged open reading frame is available. These studies have revealed that 40 nm NPs rapidly transit through Rab5-positive membranes, before being passed into acidic compartments decorated with Rab9 and Rab7. Only a minor population of the internalized NPs was detected in Rab11-positive membranes, indicating that recycling of these NPs back to the cell surface was not a preferred trafficking pathway. Finally by acquiring three-dimensional information in living cells, we provide the greatest possibility of identifying all of the particles within cells which allow us to detect relatively rare events in NP trafficking. Rare events are important observations if we are to definitively understand how NPs interact with the intracellular environment. These phenomena may have important practical consequences for identifying new routes out of the endolysosomal pathway, the appreciation of which will be essential if we are to further develop nanomaterials for efficient drug delivery in a safe manner.

MATERIALS AND METHODS

Cell Culture. All cell culture reagents were purchased from Invitrogen Corporation/Life Technologies (Carlsbad, CA) unless otherwise specified. HeLa Kyoto cells were cultured in Dulbecco's modified Eagle's medium (DMEM) with Glutamax I supplemented with 10% fetal bovine serum (FBS) and 5% penicillin/streptomycin at 37 °C and 5% CO_2.

Nanoparticles. Fluorescently labeled carboxylated polystyrene nanoparticles (PS-COOH, Invitrogen, yellow green, 40 and 100 nm) were used without further modification or purification. Nanoparticle size (hydrodynamic diameter) and surface charge (zeta-potential) were measured by dynamic light scattering (DLS) using Malvern Zetasizer Nano ZS90 (Worcestershire, UK). Freshly prepared nanoparticle dispersions were characterized in phosphate buffered saline (PBS) at 25 °C and in complete cell culture medium (cDMEM) at 37 °C. DLS results are the average of a minimum of five separate runs and are reported in Supporting Information Table S1.

Live Cell Imaging. Typically, 15 000 cells per well were seeded and grown in 4-well chambered coverglass slides (Lab-Tek II, Nunc). The LAMP1-RFP fusion construct (CellLight Lysosomes-RFP) was purchased from Invitrogen/Life Technologies and was transfected into cells according to the manufacturer's instructions. The human cDNAs encoding the RabGTPases used in this study have been described elsewhere[44] but, for the purposes of this study, were subcloned into the pmCherry-C1 vector (Clontech) to generate N-terminal mCherry fusion constructs. The mCherry-Rab constructs were transfected into cells using FuGENE6 (Roche) according to the manufacturer's instructions. All transfections were carried out approximately 24 h after

seeding, and between 15 and 24 h before imaging. Cells were washed once with PBS at 37 °C before a short pulse of exposure to a NP dispersion in cDMEM (1 min and 50 μg/mL for the 40 nm NPs and 5 min and 250 μg/mL for the 100 nm NPs). After removal of the NP dispersion, the cells were washed five times with PBS at 37 °C before adding fresh cDMEM. Cells were then imaged in a live cell imaging chamber (37 °C, 5% CO_2), using a spinning disk confocal microscopy system consisting of a CSU-X1 spinning disk unit (Yokogawa Electric Corporation) and an iXon DU-897-BV EMCCD camera (Andor), mounted on a Nikon Ti inverted microscope, with a motorized *XY* stage allowing for multiposition and a piezo stepper for fast z-sectioning. Images were acquired with a 100× oil immersion objective, NA = 1.45. Laser lines at 488 and 561 nm were used to excite the NP and RFP/mCherry fluorescence, respectively. For each field, three consecutive z-stacks (30 optical sections) were imaged at every time point.

For imaging of cells transfected with the mCherry-Rab1A construct, 65 000 cells were seeded in a 35 mm μ-dish with a grid structure (Grid-500, Ibidi). The grid structure was used to locate the cells imaged live, following fixation and immunostaining (see below). Transfection and NP (40 nm) addition was carried out as described above, and cells were imaged in our live cell setup at different time intervals after NP exposure. The time-lapse movies were acquired by taking 4−5 optical slices and 30−50 frames with a frame rate of 1−1.5 s.

Confocal Imaging and Immunofluorescence Staining. Immediately after the live cell acquisition, the cells were fixed in ice cold methanol and stained using primary mouse monoclonal antibodies against LC3 (NanoTools) followed by secondary anti-mouse antibodies coupled to Alexa647 (Molecular Probes). The grid structure in the dishes was used to locate the cells that had been imaged live. Confocal images were acquired with an Olympus FV1000 system using a 60×/NA1.35 oil immersion objective. Sequential acquisition mode was used in all cases.

Image Analysis. Masking and segmentation of the images was performed using Imaris software (Bitplane). The cell or cells in the field of view were first individually masked out to remove adjacent cells and any NPs adsorbed to the glass surface. The NPs in the masked region of the image were segmented with the "spot detection" algorithm, using a Mexican hat filter for dynamic background subtraction. The identified spots were classified and filtered using the quality filter and occasionally in combination with an intensity filter. All threshold values were set manually. LAMP1 and Rab-labeled structures were segmented with the "surface detection" algorithm also using a Mexican hat filter for dynamic background subtraction. Using the surfaces, these structures were rendered as fixed value homogeneous volumes. A NP was determined to be colocalized with the structure of interest if the center of its corresponding spot was localized within that rendered volume. The colocalization can be given as either the fraction of cell-associated NPs that are colocalized with LAMP1 or Rab structures at each time point or simply as the number of colocalized NP objects. The term "NP objects" is used since the objects that are identified as NPs when segmenting the images may contain one or several NPs, and referring to them as NPs could be misleading. When calculating the fraction of colocalized NPs, the intensity data were used to obtain a value that reflected the actual number of NPs. The results at each time point is the average of the data for the three consecutive frames acquired at each time point.

Conflict of Interest: The authors declare no competing financial interest.

Supporting Information Available: NP characterization, time traces of the colocalization between NP and different Rabs for individual cells, movie of RFP-LAMP1 and NP, and movie illustrating comovement between mCherry-Rab1A and NP. This material is available free of charge *via* the Internet at http://pubs.acs.org.

REFERENCES AND NOTES

1. Mailänder, V.; Landfester, K. Interaction of Nanoparticles with Cells. *Biomacromolecules* **2009**, *10*, 2379–2400.
2. Verma, A.; Stellacci, F. Effect of Surface Properties on Nanoparticle−Cell Interactions. *Small* **2010**, *6*, 12–21.
3. Hillaireau, H.; Couvreur, P. Nanocarriers' Entry into the Cell: Relevance to Drug Delivery. *Cell. Mol. Life Sci.* **2009**, *66*, 2873–2896.
4. Delehanty, J.; Mattoussi, H.; Medintz, I. Delivering Quantum Dots into Cells: Strategies, Progress and Remaining Issues. *Anal. Bioanal. Chem.* **2009**, *393*, 1091–1105.
5. Hild, W. A.; Breunig, M.; Goepferich, A. Quantum Dots—Nano-sized Probes for the Exploration of Cellular and Intracellular Targeting. *Eur. J. Pharm. Biopharm.* **2008**, *68*, 153–168.
6. Sahay, G.; Alakhova, D. Y.; Kabanov, A. V. Endocytosis of Nanomedicines. *J. Controlled Release* **2010**, *145*, 182–195.
7. Chithrani, B. D.; Ghazani, A. A.; Chan, W. C. W. Determining the Size and Shape Dependence of Gold Nanoparticle Uptake into Mammalian Cells. *Nano Lett.* **2006**, *6*, 662–668.
8. He, C.; Hu, Y.; Yin, L.; Tang, C.; Yin, C. Effects of Particle Size and Surface Charge on Cellular Uptake and Biodistribution of Polymeric Nanoparticles. *Biomaterials* **2010**, *31*, 3657–3666.
9. Rejman, J.; Oberle, V.; Zuhorn, I. S.; Hoekstra, D. Size-Dependent Internalization of Particles *via* the Pathways of Clathrin- and Caveolae-Mediated Endocytosis. *Biochem. J.* **2004**, *377*, 159–169.
10. Gratton, S. E. A.; Ropp, P. A.; Pohlhaus, P. D.; Luft, J. C.; Madden, V. J.; Napier, M. E.; DeSimone, J. M. The Effect of Particle Design on Cellular Internalization Pathways. *Proc. Natl. Acad. Sci. U.S.A.* **2008**, *105*, 11613–11618.
11. Yue, Z.-G.; Wei, W.; Lv, P.-P.; Yue, H.; Wang, L.-Y.; Su, Z.-G.; Ma, G.-H. Surface Charge Affects Cellular Uptake and Intracellular Trafficking of Chitosan-Based Nanoparticles. *Biomacromolecules* **2011**, *12*, 2440–2446.
12. Lunov, O.; Syrovets, T.; Loos, C.; Beil, J.; Delacher, M.; Tron, K.; Nienhaus, G. U.; Musyanovych, A.; Mailänder, V.; Landfester, K.; *et al.* Differential Uptake of Functionalized Polystyrene Nanoparticles by Human Macrophages and a Monocytic Cell Line. *ACS Nano* **2011**, *5*, 1657–1669.
13. Douglas, K. L.; Piccirillo, C. A.; Tabrizian, M. Cell Line-Dependent Internalization Pathways and Intracellular Trafficking Determine Transfection Efficiency of Nanoparticle Vectors. *Eur. J. Pharm. Biopharm.* **2008**, *68*, 676–687.
14. Lorenz, M. R.; Holzapfel, V.; Musyanovych, A.; Nothelfer, K.; Walther, P.; Frank, H.; Landfester, K.; Schrezenmeier, H.; Mailänder, V. Uptake of Functionalized, Fluorescent-Labeled Polymeric Particles in Different Cell Lines and Stem Cells. *Biomaterials* **2006**, *27*, 2820–2828.
15. Lai, S. K.; Hida, K.; Man, S. T.; Chen, C.; Machamer, C.; Schroer, T. A.; Hanes, J. Privileged Delivery of Polymer Nanoparticles to the Perinuclear Region of Live Cells *via* a Non-clathrin, Non-degradative Pathway. *Biomaterials* **2007**, *28*, 2876–2884.
16. Tekle, C.; van Deurs, B.; Sandvig, K.; Iversen, T.-G. Cellular Trafficking of Quantum Dot-Ligand Bioconjugates and Their Induction of Changes in Normal Routing of Unconjugated Ligands. *Nano Lett.* **2008**, *8*, 1858–1865.
17. Cedervall, T.; Lynch, I.; Lindman, S.; Berggård, T.; Thulin, E.; Nilsson, H.; Dawson, K. A.; Linse, S. Understanding the Nanoparticle−Protein Corona Using Methods To Quantify

Exchange Rates and Affinities of Proteins for Nanoparticles. *Proc. Natl. Acad. Sci. U.S.A.* **2007**, *104*, 2050–2055.

18. Lundqvist, M.; Stigler, J.; Elia, G.; Lynch, I.; Cedervall, T.; Dawson, K. A. Nanoparticle Size and Surface Properties Determine the Protein Corona with Possible Implications for Biological Impacts. *Proc. Natl. Acad. Sci. U.S.A.* **2008**, *105*, 14265–14270.

19. Monopoli, M. P.; Walczyk, D.; Campbell, A.; Elia, G.; Lynch, I.; Baldelli Bombelli, F.; Dawson, K. A. Physical−Chemical Aspects of Protein Corona: Relevance to *In Vitro* and *In Vivo* Biological Impacts of Nanoparticles. *J. Am. Chem. Soc.* **2011**, *133*, 2525–2534.

20. Walczyk, D.; Bombelli, F. B.; Monopoli, M. P.; Lynch, I.; Dawson, K. A. What the Cell "Sees" in Bionanoscience. *J. Am. Chem. Soc.* **2010**, *132*, 5761–5768.

21. Bacallao, R.; Sohrab, S.; Phillips, C. Guiding Principles of Specimen Preservation for Confocal Fluorescence Microscopy. In *Handbook Of Biological Confocal Microscopy*; Pawley, J. B., Ed.; Springer Science: New York, 2006; pp 368−380.

22. Vercauteren, D.; Deschout, H.; Remaut, K.; Engbersen, J. F. J.; Jones, A. T.; Demeester, J.; De Smedt, S. C.; Braeckmans, K. Dynamic Colocalization Microscopy To Characterize Intracellular Trafficking of Nanomedicines. *ACS Nano* **2011**, *5*, 7874–7884.

23. Salvati, A.; Åberg, C.; dos Santos, T.; Varela, J.; Pinto, P.; Lynch, I.; Dawson, K. A. Experimental and Theoretical Comparison of Intracellular Import of Polymeric Nanoparticles and Small Molecules: Toward Models of Uptake Kinetics. *Nanomedicine* **2011**, *7*, 818–826.

24. Lesniak, A.; Campbell, A.; Monopoli, M. P.; Lynch, I.; Salvati, A.; Dawson, K. A. Serum Heat Inactivation Affects Protein Corona Composition and Nanoparticle Uptake. *Biomaterials* **2010**, *31*, 9511–9518.

25. Conner, S. D.; Schmid, S. L. Regulated Portals of Entry into the Cell. *Nature* **2003**, *422*, 37–44.

26. McMahon, H. T.; Boucrot, E. Molecular Mechanism and Physiological Functions of Clathrin-Mediated Endocytosis. *Nat. Rev. Mol. Cell Biol.* **2011**, *12*, 517–533.

27. Luzio, J. P.; Pryor, P. R.; Bright, N. A. Lysosomes: Fusion and Function. *Nat. Rev. Mol. Cell Biol.* **2007**, *8*, 622–632.

28. Stenmark, H. Rab GTPases as Coordinators of Vesicle Traffic. *Nat. Rev. Mol. Cell Biol.* **2009**, *10*, 513–525.

29. Behnia, R.; Munro, S. Organelle Identity and the Signposts for Membrane Traffic. *Nature* **2005**, *438*, 597–604.

30. Sönnichsen, B.; De Renzis, S.; Nielsen, E.; Rietdorf, J.; Zerial, M. Distinct Membrane Domains on Endosomes in the Recycling Pathway Visualized by Multicolor Imaging of Rab4, Rab5, and Rab11. *J. Cell. Biol.* **2000**, *149*, 901–914.

31. Feng, Y.; Press, B.; Wandinger-Ness, A. Rab 7: An Important Regulator of Late Endocytic Membrane Traffic. *J. Cell. Biol.* **1995**, *131*, 1435–1452.

32. Vanlandingham, P. A.; Ceresa, B. P. Rab7 Regulates Late Endocytic Trafficking Downstream of Multivesicular Body Biogenesis and Cargo Sequestration. *J. Biol. Chem.* **2009**, *284*, 12110–12124.

33. Rink, J.; Ghigo, E.; Kalaidzidis, Y.; Zerial, M. Rab Conversion as a Mechanism of Progression from Early to Late Endosomes. *Cell* **2005**, *122*, 735–749.

34. Lombardi, D.; Soldati, T.; Riederer, M. A.; Goda, Y.; Zerial, M.; Pfeffer, S. R. Rab9 Functions in Transport between Late Endosomes and the Trans Golgi Network. *EMBO J.* **1993**, *12*, 667–682.

35. Barbero, P.; Bittova, L.; Pfeffer, S. R. Visualization of Rab9-Mediated Vesicle Transport from Endosomes to the Trans-Golgi in Living Cells. *J. Cell. Biol.* **2002**, *156*, 511–518.

36. Ullrich, O.; Reinsch, S.; Urbé, S.; Zerial, M.; Parton, R. G. Rab11 Regulates Recycling through the Pericentriolar Recycling Endosome. *J. Cell. Biol.* **1996**, *135*, 913–924.

37. Kim, J. A.; Åberg, C.; Salvati, A.; Dawson, K. A. Role of Cell Cycle on the Cellular Uptake and Dilution of Nanoparticles in a Cell Population. *Nat. Nanotechnol.* **2012**, *7*, 62–68.

38. Shapero, K.; Fenaroli, F.; Lynch, I.; Cottell, D. C.; Salvati, A.; Dawson, K. A. Time and Space Resolved Uptake Study of Silica Nanoparticles by Human Cells. *Mol. BioSyst.* **2011**, *7*, 371–378.

39. Davidson, H. W.; Balch, W. E. Differential Inhibition of Multiple Vesicular Transport Steps between the Endoplasmic Reticulum and Trans Golgi Network. *J. Biol. Chem.* **1993**, *268*, 4216–4226.

40. Lee, M. C. S.; Miller, E. A.; Goldberg, J.; Orci, L.; Schekman, R. Bi-directional Protein Transport between the ER and Golgi. *Annu. Rev. Cell Dev. Biol.* **2004**, *20*, 87–123.

41. Carlos Martín Zoppino, F.; Damián Militello, R.; Slavin, I.; Álvarez, C.; Colombo, M. I. Autophagosome Formation Depends on the Small GTPase Rab1 and Functional ER Exit Sites. *Traffic* **2010**, *11*, 1246–1261.

42. Zabirnyk, O.; Yezhelyev, M.; Seleverstov, O. Nanoparticles as a Novel Class of Autophagy Activators. *Autophagy* **2007**, *3*, 278–281.

43. Mukhopadhyay, A.; Nieves, E.; Che, F.-Y.; Wang, J.; Jin, L.; Murray, J. W.; Gordon, K.; Angeletti, R. H.; Wolkoff, A. W. Proteomic Analysis of Endocytic Vesicles: Rab1a Regulates Motility of Early Endocytic Vesicles. *J. Cell Sci.* **2011**, *124*, 765–775.

44. Simpson, J. C.; Griffiths, G.; Wessling-Resnick, M.; Fransen, J. A. M.; Bennett, H.; Jones, A. T. A Role for the Small GTPase Rab21 in the Early Endocytic Pathway. *J. Cell Sci.* **2004**, *117*, 6297–6311.